Partition Model–Based ^{99m}Tc-MAA SPECT/CT Predictive Dosimetry Compared with ^{90}Y TOF PET/CT Posttreatment Dosimetry in Radioembolization of Hepatocellular Carcinoma: A Quantitative Agreement Comparison

Silvano Gnesin*[1], Laurent Canetti*[1], Salim Adib[2], Nicolas Cherbuin[1], Marina Silva Monteiro[2], Pierre Bize[3], Alban Denys[3], John O. Prior[2], Sebastien Baechler[1], and Ariane Boubaker[2]

[1]Institute of Radiation Physics, Lausanne University Hospital, Lausanne, Switzerland; [2]Nuclear Medicine and Molecular Imaging Department, Lausanne University Hospital, Lausanne, Switzerland; and [3]Radiology Department, Lausanne University Hospital, Lausanne, Switzerland

^{90}Y-microsphere selective internal radiation therapy (SIRT) is a valuable treatment in unresectable hepatocellular carcinoma (HCC). Partition-model predictive dosimetry relies on differential tumor-to-nontumor perfusion evaluated on pretreatment ^{99m}Tc-macroaggregated albumin (MAA) SPECT/CT. The aim of this study was to evaluate agreement between the predictive dosimetry of ^{99m}Tc-MAA SPECT/CT and posttreatment dosimetry based on ^{90}Y time-of-flight (TOF) PET/CT. **Methods:** We compared the ^{99m}Tc-MAA SPECT/CT results for 27 treatment sessions (25 HCC patients, 41 tumors) with ^{90}Y SIRT (7 glass spheres, 20 resin spheres) and the posttreatment ^{90}Y TOF PET/CT results. Three-dimensional voxelized dose maps were computed from the ^{99m}Tc-MAA SPECT/CT and ^{90}Y TOF PET/CT data. Mean absorbed dose (D_{mean}) was evaluated to compute the predicted-to-actual dose ratio ($DR_{mean} = D^{MAA}_{mean}/D^{90Y}_{mean}$) in tumor volumes (TVs) and nontumor volumes (NTVs) for glass and resin spheres. The Lin concordance (ρ_c) was used to measure accuracy (C_b) and precision (ρ). **Results:** Administered activity ranged from 0.8 to 1.9 GBq for glass spheres and from 0.6 to 3.4 GBq for resin spheres, and the respective TVs ranged from 2 to 125 mL and from 6 to 1,828 mL. The mean dose D^{90Y}_{mean} was 240 Gy for glass and 122 Gy for resin in TVs and 72 Gy for glass and 47 Gy for resin in NTVs. DR^{TV}_{mean} was 1.46 ± 0.58 (0.65–2.53) for glass and 1.16 ± 0.41 (0.54–2.54) for resin, and the respective values for DR^{NTV}_{mean} were 0.88 ± 0.15 (0.56–1.00) and 0.86 ± 0.2 (0.58–1.35). DR variability was substantially lower in NTVs than in TVs. The Lin concordance between D^{MAA}_{mean} and D^{90Y}_{mean} (resin) was significantly better for tumors larger than 150 mL than for tumors 150 mL or smaller ($\rho_c = 0.93$ and $C_b = 0.95$ vs. $\rho_c = 0.57$ and $C_b = 0.93$; $P < 0.05$). **Conclusion:** In ^{90}Y radioembolization of HCC, predictive dosimetry based on ^{99m}Tc-MAA SPECT/CT provided good estimates of absorbed doses calculated from posttreatment ^{90}Y TOF PET/CT for tumor and nontumor tissues. The low variability of DR^{NTV} demonstrates that pretreatment dosimetry is particularly suitable for minimizing radiation-induced hepatotoxicity.

Received Jan. 25, 2016; revision accepted May 16, 2016.

For correspondence or reprints contact: Silvano Gnesin, Institute of Radiation Physics, Lausanne University Hospital, Rue du Grand-Pré 1, CH-1007 Lausanne, Switzerland.

E-mail: silvano.gnesin@chuv.ch

*Contributed equally to this work.

Published online Jun. 15, 2016.

Key Words: selective internal radiation therapy (SIRT); ^{90}Y radioembolization; predictive dosimetry; hepatocellular carcinoma (HCC)

J Nucl Med 2016; 57:1672–1678
DOI: 10.2967/jnumed.116.173104

In selective internal radiation therapy (SIRT), ^{90}Y-microsphere radioembolization is a valuable therapeutic option in patients presenting with unresectable hepatocellular carcinoma (HCC) not eligible for other therapeutic options (*1–3*).

SIRT with ^{90}Y-charged microspheres relies on differential vascularization between tumor and nontumor liver parenchyma, resulting in favorable, potentially tumoricidal, deposition of microsphere activity in tumors while minimizing absorbed dose to the functional parenchyma, thus preventing toxicity. Two microsphere types are clinically available: resin spheres (SIR spheres; SirTex Medical Ltd.) and glass spheres (TheraSphere; Nordion Inc.). Despite being of similar size (~30 μm), these two types of sphere differ in specific activity, density ($\cong 4 \times 10^5$ glass spheres/GBq; $\cong 2 \times 10^7$ resin spheres/GBq), and injection solution (NaCl for glass spheres; water for resin spheres), leading to potential differences in embolic effect and local variations in the radiation dose deposited in tissues.

Predictive dosimetry has included hepatic CT angiography for catheter positioning and partition modeling based on ^{99m}Tc-macroaggregate albumin (MAA) SPECT/CT acquisition (*4,5*).

The manufacturer-recommended activity for resin spheres is based on a semiempiric formula including body surface area (*6,7*) and tumor burden. This approach can be refined using a 3-compartment partition model (*4*) including the lungs, liver TVs, and liver NTVs derived from a pretreatment ^{99m}Tc-MAA SPECT/CT scan. The prescribed glass sphere activity is based on a 2-compartment model (lungs and targeted liver regions) aiming to deliver a dose of 80–150 Gy to the targeted liver volume.

^{90}Y time-of-flight (TOF) PET/CT dosimetry (*8*) provides a valuable tool to verify ^{99m}Tc-MAA SPECT/CT–based predictive dosimetry.

Accurate TV and NTV predictive dosimetry is essential for patient safety, good tumor control with low hepatic toxicity, and evaluation of the dose response. The predictive value of ^{99m}Tc-MAA SPECT/CT–based dosimetry is debated (*9,10*). In hepatic metastases from colorectal cancer, Flamen et al. (*11*) observed that metabolic response using total tumor glycolysis correlated well with ^{99m}Tc-MAA–predicted dose. In contrast, Wondergem et al. (*12*) reported poor agreement between ^{99m}Tc-MAA SPECT/CT–evaluated activity distribution and posttreatment bremsstrahlung SPECT/CT findings; these results were debated by Kao (*13*). In HCC patients treated with glass spheres, Garin et al. (*14*) reported that ^{99m}Tc-MAA SPECT/CT accurately predicted tumor response and survival. Kao et al. (*15*) reported a good dose–response correlation and reliable predictive dosimetry for ^{99m}Tc-MAA SPECT/CT compared with posttreatment ^{90}Y TOF PET in HCC patients treated with resin spheres. Postradioembolization ^{90}Y TOF PET/CT can also provide valuable information in cases of extrahepatic shunt (*16*), helping the physician take appropriate corrective actions and improving posttherapy patient management.

We aimed to evaluate agreement between ^{99m}Tc-MAA SPECT/CT–based predictive dosimetry and posttreatment ^{90}Y TOF PET/CT–based dosimetry for both TV and NTV in HCC patients treated with both resin and glass spheres. To our knowledge, this is the first report assessing and comparing both devices in patients treated at the same institution using the same clinical procedure.

MATERIALS AND METHODS

All procedures were performed in accordance with the ethical standards of the institutional and national research committee and with the Declaration of Helsinki. Informed consent was obtained from individual participants before study inclusion.

Cohort Description

We retrospectively compared 27 treatment sessions on 25 HCC patients (Table 1) who underwent ^{90}Y SIRT between May 2012 and November 2013. Sequential SIRT whole-liver sessions ($n = 1$) and lobar-plus-segmentectomy sessions ($n = 1$) at 2- and 7-mo intervals were considered as distinct procedures. In total, there were 20 lobar (17 right and 3 left), 2 whole-liver, 2 lobar-with-segment-boost, 2 segment, and 1 partial-lobe treatments. In total, 41 tumors (TV) were identified and analyzed.

According to the Barcelona Clinic liver cancer classification, 3 patients had stage A disease, 14 had stage B, and 8 had stage C. Only one patient had a normal liver; all others had cirrhotic liver disease (16 Child–Pugh A, 6 B, and 2 C). Lobar or sectorial portal vein thrombosis was present in 7 patients. Among the 25 patients, 11 were treatment-naive and 14 had already undergone various procedures before radioembolization (5 hepatectomy or segmentectomy, 8 chemoembolization, and 6 radiofrequency ablation or thermoablation). Seven treatments (11 tumors) were performed with glass spheres and 20 (30 tumors) with resin spheres; details are summarized in Table 1.

Patients with small TVs (≤150 mL) were preferentially treated with ^{90}Y-glass spheres because of their higher specific activity and lower particle number, aiming at avoiding tumor saturation and consequent reflux to nontarget volumes. All tumors treated with glass spheres were 150 mL or smaller, whereas tumors selected for resin spheres had a wider range of volume (6–1,828 mL).

Activity Determination

Resin sphere dosimetry is based on a 3-compartment partition model aiming at keeping the dose to the NTV below 70 Gy and 50 Gy for lobar and total liver treatment, respectively, as recommended by Lau et al. (*7*).

Determination of glass sphere activity is based on a 2-compartment model (lungs plus targeted liver region) aiming at delivering a dose of between 80 and 150 Gy to the targeted liver volume. In analogy with the resin sphere dosimetry, we refined the activity determination by applying as a second step a partition model accounting for TV and NTV and differential particle distribution (tumor-to-nontumor ratio) estimated from ^{99m}Tc-MAA SPECT/CT to predict TV and NTV dose. In lobar radioembolization, we keep the average predicted NTV dose to below 70 Gy provided this allows a predicted tumor dose of more than 205 Gy (*14*).

Pretherapy ^{99m}Tc-MAA SPECT/CT

Hepatic angiography was performed, and after occluding single or multiple accessory hepatic arteries (when present) with coils, 120–180 MBq of ^{99m}Tc-MAA in 5 mL of physiologic solution were slowly administrated via the catheter, the exact position of which was noted and registered on the angiogram to guide catheter repositioning for the treatment session.

The patient was immediately (<20 min) transferred to the nuclear medicine department for SPECT/CT, with whole-body and planar images being acquired within 1 h for evaluation of lung shunting. Abdominal SPECT/CT images (Discovery 670/Infinia Hawkeye IV; GE Healthcare) were acquired (120 × 20 s, low-energy high-resolution collimator) and reconstructed with a Xeleris 3.1 workstation (GE Healthcare) using 3-dimensional (3D) ordered-subset expectation maximization (4 iterations × 10 subsets) with a Butterworth filter (cutoff, 0.5 cycles/cm; order, 10) and CT-based attenuation correction. The TV, NTV, and tumor-to-nontumor ratio were assessed on the SPECT/CT images, with morphologic information obtained from any available imaging modality (enhanced CT, MR, or ^{18}F-FDG PET/CT) when needed.

TABLE 1
Patient Age, Administered Activity, TVs, and NTVs for Glass and Resin Spheres

		Administered activity (GBq)		TV (mL)		NTV (mL)	
Parameter	Patient age (y)	Glass	Resin	Glass	Resin	Glass	Resin
Minimum	43	0.8	0.6	2	6	298	278
Maximum	87	1.9	3.4	125	1,828	1,295	2,345
Mean	66	1.3	1.9	34	359	724	1,120
SD	11	0.4	0.9	38	501	383	574

Posttherapeutic ^{90}Y TOF PET

The required activity in gigabecquerels determined from ^{99m}Tc-MAA dosimetry was administered according to the manufacturer's instructions. The injected activity was measured, as well as the post-procedural activity in the delivery system and catheters. The actual (i.e., gold standard) dose absorbed by tissue was quantified from posttreatment ^{90}Y TOF PET/CT performed within 6 h after ^{90}Y-sphere administration (Discovery 690; GE Healthcare) (*17*). The PET acquisition duration was 30 min per bed position, for 1 or 2 bed positions depending on the axial dimension of the liver. The list-mode acquisition integrating TOF data was reconstructed using 3D ordered-subset expectation maximization (VPFX [GE Healthcare], 2 iterations × 16 subsets) including a gaussian postreconstruction filter of 5 mm in full width at half maximum. All image corrections (normalization, dead time, activity decay, random coincidences, attenuation, and scatter) were applied.

Image Segmentation, Volume-of-Interest Definition, and Dosimetry

PMOD software (release 3.4; PMOD Technologies Ltd.) was used for coregistration of ^{90}Y TOF PET and ^{99m}Tc-MAA SPECT images with CT or MR images and for manual or semiautomatic (threshold) delineation of TVs and NTVs by the nuclear medicine physician and technologist.

TVs, NTVs, and tumor-to-nontumor ratios estimated from the ^{99m}Tc-MAA SPECT images using partition model dosimetry were applied to determine the activity of ^{90}Y-spheres to be administered (*18*). For each procedure, 3D voxelized ^{90}Y dose maps were computed from the ^{99m}Tc-MAA SPECT/CT and ^{90}Y TOF PET/CT acquisitions with assumption of local energy deposition (*19*), which considers the measured voxel activity to contribute to the absorbed dose in only the voxel itself. Permanent sphere implantation was also assumed. We performed a phantom study to determine the accuracy of total-activity recovery in ^{90}Y PET acquisitions. For that purpose, a Kyoto liver phantom (1.8-L liver volume) was used. Even when our PET scanner was calibrated to measure ^{90}Y emission quantitatively, we found 5%–10% deviations compared with the actual total activity in the phantom. Thus, we preferred to rescale the total PET signal to the activity administered to improve the accuracy of total-activity recovery.

The total therapeutic administered activity was partitioned proportionally to the relative voxel intensity to derive both predictive SPECT and posttreatment PET 3D activity maps in units of kBq/mL. The 3D voxelized dose map was then obtained by rescaling the activity map by a factor 49.67 Gy/(GBq/kg) (*20,21*). Dose–volume histograms for both TV and NTV were obtained. Average absorbed doses in tumors were corrected for partial-volume effects through multiplication by appropriate recovery coefficients according to tumor size, estimated by phantom measurements with both the ^{90}Y TOF PET and the ^{99m}Tc-SPECT modalities (Supplemental Fig. 1; supplemental materials are available at http://jnm.snmjournals.org).

Data Analysis

Dose maps allowed us to define, for each volume of interest, the mean ^{90}Y dose computed from ^{99m}Tc-MAA SPECT (D^{MAA}_{mean}) and from ^{90}Y TOF PET (D^{90Y}_{mean}) and a predicted-to-actual dose ratio:

$$DR^{VOI}_{mean} = D^{MAA}_{mean}|_{VOI} / D^{90Y}_{mean}|_{VOI}. \quad \text{Eq. 1}$$

This ratio has a clear interpretation: for values of DR^{VOI} less than 1, predictive dosimetry underestimates mean absorbed dose, whereas for values of DR^{VOI} greater than 1, mean absorbed dose is overestimated.

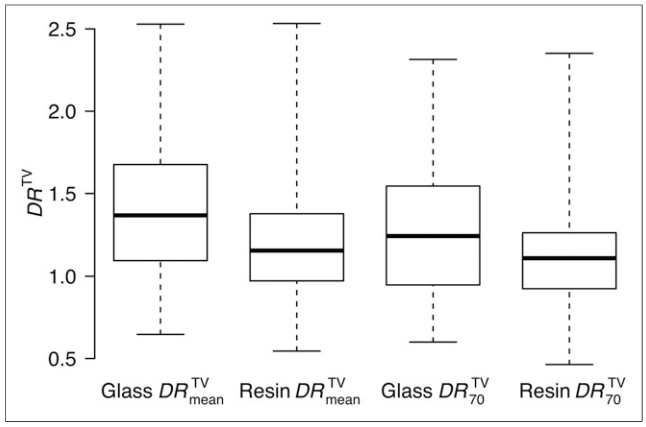

FIGURE 1. Box plot of ^{90}Y predicted-to-actual dose ratios DR^{TV}_{mean} and DR^{TV}_{70} in TVs for both resin and glass spheres, as defined in Equation 1.

The value derived from the dose–volume histogram representing the minimum absorbed dose delivered to 70% of the target volume (the 70th percentile dose [D_{70}]) was evaluated from ^{99m}Tc-MAA SPECT (D^{MAA}_{70}) and from ^{90}Y TOF PET (D^{90Y}_{70}); this estimator has recently been used to characterize dose response in SIRT (*15*). The values of D^{MAA}_{70} and D^{90Y}_{70} were evaluated for TV and NTV. To assess agreement between $D^{MAA}_{mean\ or\ 70}$ and $D^{90Y}_{mean\ or\ 70}$ distributions, we use the Lin concordance coefficient (*22*), ρ_c:

$$\rho_c = \rho C_b, \quad \text{Eq. 2}$$

where ρ ($\in [-1, 1]$) is the Pearson correlation coefficient of the linear relationship between the data (precision) whereas C_b ($\in [0, 1]$) is a bias coefficient, which measures departure of the best-fit curve from the 45° line (accuracy).

RESULTS

We compared the predictive dosimetry from the ^{99m}Tc-MAA SPECT–derived dose map with the posttreatment dosimetry obtained from the ^{90}Y TOF PET dose map for TVs and NTVs.

TABLE 2
Tumor Predicted Doses D^{MAA}_{70}, Absorbed Doses D^{MAA}_{mean}, and Their Ratio for Glass and Resin Spheres

	D^{MAA}(Gy)		D^{90Y}(Gy)		DR^{TV}	
Parameter	Glass	Resin	Glass	Resin	Glass	Resin
Mean dose (D_{mean})						
Minimum	150	38	99	38	0.65	0.54
Maximum	583	287	471	329	2.53	2.54
Mean	321	129	240	122	1.46	1.16
70th percentile dose (D_{70})						
Minimum	173	45	121	48	0.60	0.46
Maximum	563	301	563	406	2.32	2.35
Mean	355	151	297	143	1.31	1.14

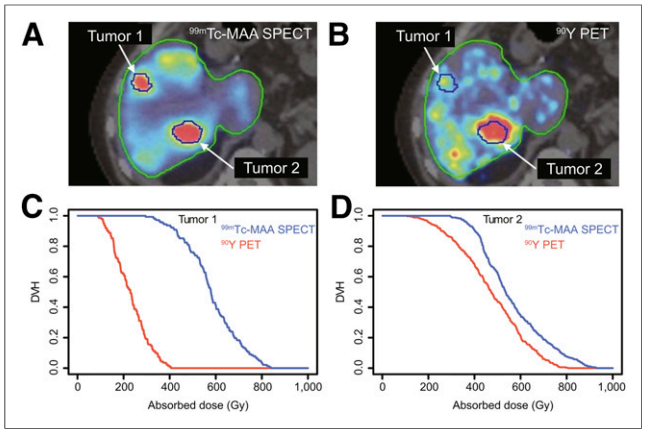

FIGURE 2. (A and B) ^{99m}Tc-MAA SPECT (A) and ^{90}Y TOF PET (B) images of liver treated with glass spheres, with treated volume delimited by green lines and tumors by blue lines. (C and D) Dose–volume histograms (DVH) of tumors 1 (C) and 2 (D), with blue lines corresponding to ^{90}Y dosimetry based on ^{99m}Tc-MAA SPECT spatial distribution and red lines to ^{90}Y TOF PET (posttreatment dosimetry).

TABLE 3
Volumes and Doses for TVs of Figure 2 and Supplemental Figure 2

Sphere type	Volume (mL)	D^{MAA}_{mean} (Gy)	D^{90Y}_{mean} (Gy)	DR^{TV}_{mean}
Glass				
Tumor 1	3	583	230	2.53
Tumor 2	8	564	471	1.20
Resin	539	132	113	1.16

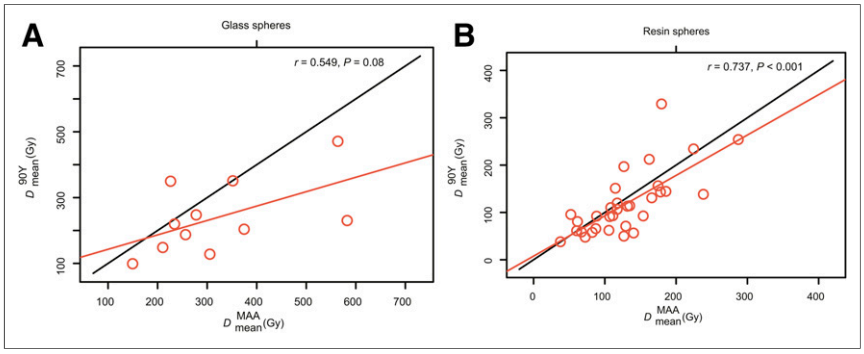

FIGURE 3. Comparison of mean tumor dose (D_{mean}) between predictive ^{90}Y dosimetry based on ^{99m}Tc-MAA SPECT and posttreatment dosimetry based on ^{90}Y TOF PET for glass (A) and resin (B) spheres. Diagonal red lines indicate linear regression fitted with least-squares method; diagonal black line indicates perfect concordance.

Tumor

The average, minimum, and maximum values of mean tumor doses D_{mean} and D_{70} and tumor dose ratios DR^{TV}_{mean} and DR^{TV}_{70} are summarized according to the specific therapeutic approach (glass spheres [11 tumors] and resin spheres [30 tumors]) in Figure 1 and Table 2.

D_{mean} and D_{70} quantifications gave comparable results. Overall, DR^{TV} values indicated a trend for the predictive dosimetry to overestimate the dose as obtained from posttreatment ^{90}Y TOF PET–derived dose maps. In particular, our results showed a large variability of DR^{TV}. In specific patients, for both glass and resin therapeutic approaches, we found DR^{TV} values as low as 0.6 and as high as 2.5. This result quantitatively describes the extent of diametric uncertainty when using ^{99m}Tc-MAA SPECT/CT for tumor predictive dosimetry. The dosimetric uncertainty for tumor is less (i.e., better) for resin spheres than for glass spheres as evidenced by the DR^{TV} distribution in Figure 1.

An example of liver treated with glass spheres and an example of liver treated with resin spheres are shown in Figure 2 and Supplemental Figure 2, respectively. Figure 2 shows glass sphere SIRT, with a TV of 1,350 mL and a 1.7-GBq administered activity. Two tumors are visible, one of which is representative of poor quantitative agreement (tumor 1, $DR^{TV}_{mean} = 2.53$) and the other of good quantitative agreement (tumor 2, $DR^{TV}_{mean} = 1.20$) between predictive and posttreatment dosimetry. TVs, mean predicted doses, mean absorbed doses, and dose ratios are listed in Table 3. Poor and good quantitative agreement between predictive and posttreatment dosimetry are also evidenced in the dose–volume histograms (Figs. 2C and 2D).

The comparison between predicted and posttreatment tumor doses, D_{mean}, is presented in Figure 3, which reports the results for glass spheres and resin spheres separately. The Lin concordance for each specific case is summarized in Table 4. Overall, concordance was better for resin spheres than for glass spheres. Glass sphere concordance was higher for D_{70} than for D_{mean} because of the higher accuracy (C_b) characterizing the D_{70} quantification.

The tumor DR^{TV} distribution as a function of TV is shown in Figure 4. We separately analyzed the DR^{TV} values obtained for resin spheres as a function of TV. As summarized in Figure 5, we found a larger DR^{TV} variability in smaller tumors (≤150 mL, 16/30 TV) than in larger tumors (>150 mL, 14/30 TV). When we compared this last result with the DR^{TV} distribution obtained for the glass sphere approach (as shown in Fig. 1), we found that the

TABLE 4
Lin Concordance Coefficients, in TV, Between Predictive Dosimetry Based on ^{99m}Tc-MAA SPECT and Posttreatment Dosimetry Based on ^{90}Y TOF PET for D_{mean} and D_{70} for Both Types of Microsphere (Fig. 4)

	Precision (ρ)		Accuracy (C_b)		Concordance (ρ_c)	
Sphere type	D_{mean}	D_{70}	D_{mean}	D_{70}	D_{mean}	D_{70}
Glass	0.55	0.58	0.79	0.91	0.44	0.53
Resin	0.72	0.68	0.97	0.97	0.69	0.65

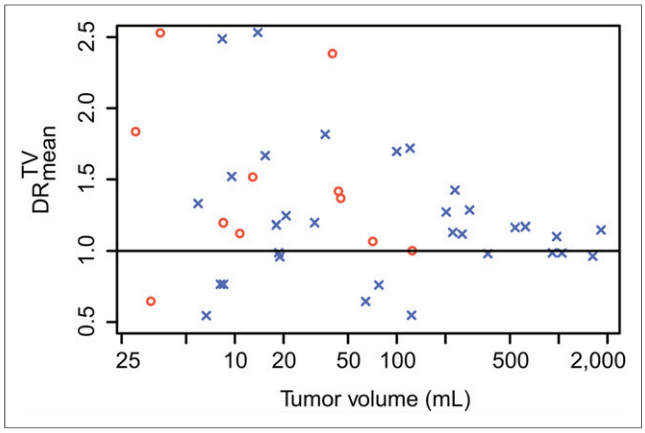

FIGURE 4. Predicted-to-actual dose ratio DR^{TV} as function of TV for glass spheres (red dots) and resin spheres (blue crosses).

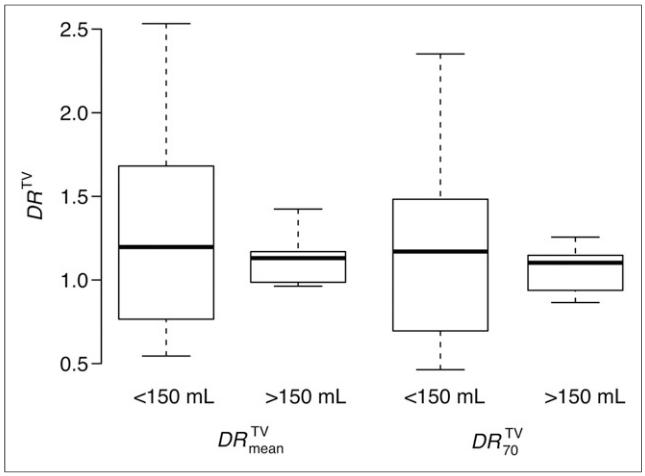

FIGURE 5. Box plot of predicted-to-actual dose ratios DR^{TV}_{mean} and DR^{TV}_{70} in TVs for resin spheres.

tumor DR^{TV} variability for tumors 150 mL or smaller was similar regardless of the sphere type.

The comparison between predicted and posttreatment dosimetry in terms of D_{mean} for the two cases—resin spheres 150 mL or smaller and resin spheres larger than 150 mL—is reported in Supplemental Figure 3. The Lin concordance for these two cases is presented in Table 5. Regardless of the quantification matrix (D_{mean} or D_{70}), we found similar accuracy for both cases, whereas better precision was found for TVs larger than 150 mL, resulting in better concordance compared with TVs of 150 mL or less.

TABLE 5
Lin Concordance Coefficients, in TV, Between Predictive Dosimetry Based on ^{99m}Tc-MAA SPECT and Posttreatment Dosimetry Based on ^{90}Y TOF PET for D_{mean} and D_{70} for Resin Microspheres (Fig. 7)

	Precision (ρ)		Accuracy (C_b)		Concordance (ρ_c)	
TV (mL)	D_{mean}	D_{70}	D_{mean}	D_{70}	D_{mean}	D_{70}
≤150	0.61	0.55	0.93	0.92	0.57	0.51
>150	0.98	0.97	0.95	0.99	0.93	0.96

NTVs

The comparison between predictive and posttreatment dosimetry in NTV was based on 27 treatments, with glass spheres (7/27 treatments) and resin spheres (20/27 treatments) being analyzed separately. In NTV, the average dose (glass or resin) from predictive and posttreatment dosimetry and the averaged dose ratios are summarized in Table 6. The DR^{NTV} distribution is reported as a box plot in Figure 6. We observed reduced DR^{NTV} variability for lower TV/NTV ratios, as was the case for patients treated with glass spheres. The comparison of D_{mean} based on predictive ^{99m}Tc-MAA SPECT versus posttreatment ^{90}Y TOF PET–derived dose maps is reported in Figure 7. The Lin concordance in NTV is presented in Table 7.

For both glass and resin spheres, concordance was very good: $\rho_{c,glass} = 0.97$ and $\rho_{c,resin} = 0.86$ for D_{mean}; $\rho_{c,glass} = 0.99$ and $\rho_{c,resin} = 0.85$ for D_{70}.

Supplemental Figure 4 shows DR^{NTV} as a function of the TV/NTV ratio. For large TV/NTV values, there was a tendency toward underestimation of predictive dose versus posttreatment dose.

DISCUSSION

Tumor Dosimetry and TVs

Predictive ^{90}Y dosimetry of tumors based on ^{99m}Tc-MAA SPECT agreed well overall with posttherapy dosimetry based on ^{90}Y TOF PET, with a tendency for predictive dosimetry to overestimate posttherapy dosimetry ($DR^{TV}_{mean} > 1$) for both resin spheres and glass spheres. We observed a large DR^{TV} variability, especially for small TVs (≤150 mL).

Our result agrees with similar observations made by Kao et al. (*15*) based on lower tumor statistics and valid only for resin spheres. In specific patients, we found tumors whose DR^{TV} were as low as 0.6 or as high as 2.5. Some possible causes of disagreement include different kinetics between ^{99m}Tc-MAA and spheres, modified tumor vascularization, and inability to perfectly reproduce the position of the catheter between ^{99m}Tc-MAA deposition and ^{90}Y-sphere administration (*12*). Other sources of measured DR^{TV} variability are differences between the PET and SPECT modalities (image resolution, noise level, contrast, and partial-volume effect). We tried to reduce variability in partial-volume effect by correcting estimated tumor activity using phantom-derived recovery coefficients. Nevertheless, the remaining variability seems to affect small TVs more severely than large ones. Statistical Lin analysis in tumors showed comparable concordance (ρ_c) for both D_{mean} and D_{70} quantification regardless of the therapeutic device (glass or resin spheres) or tumor size. Better concordance was found for resin sphere dosimetry than for glass sphere dosimetry (Fig. 3; Table 4). This finding could be due to bias, as the glass spheres were specifically chosen for small tumors (TV ≤ 150 mL) in the lobar or segment approach.

We found comparable concordance between the two types of spheres for TVs of 150 mL or less. The higher concordance found for TVs larger than 150 mL (Table 5) is explained by a better precision (ρ), whereas the accuracy ($C_b > 0.9$) did not change appreciably with tumor size, confirming the robustness of our approach.

TABLE 6
Nontumor Predicted Doses D^{MAA}, Absorbed Doses D^{90Y}, and Their Ratio DR^{NTV} for Glass and Resin Spheres

Parameter	D^{MAA} (Gy)		D^{90Y} (Gy)		DR^{NTV}	
	Glass	Resin	Glass	Resin	Glass	Resin
Mean dose (D_{mean})						
Minimum	15	17	27	17	0.56	0.58
Maximum	111	116	112	154	1.00	1.35
Mean	66	39	72	47	0.88	0.86
70th percentile dose (D_{70})						
Minimum	14	14	17	18	0.82	0.39
Maximum	142	143	153	190	0.98	1.44
Mean	83	48	87	57	0.94	0.90

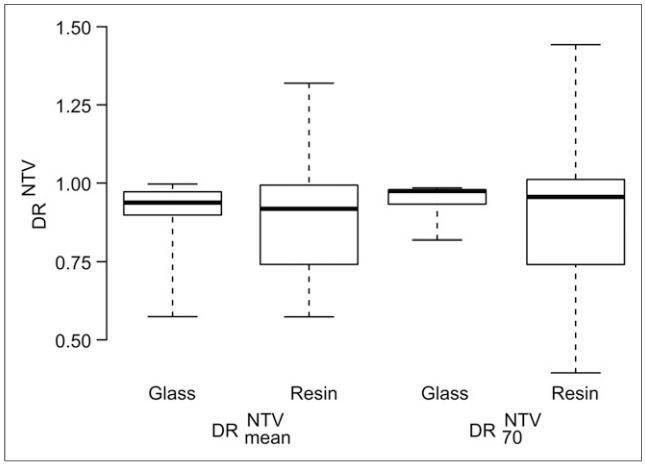

FIGURE 6. Box plot of predicted-to-actual dose ratios DR^{NTV}_{mean} and DR^{NTV}_{70} in NTV for both resin sphere and glass sphere treatment sessions, as defined in Equation 1.

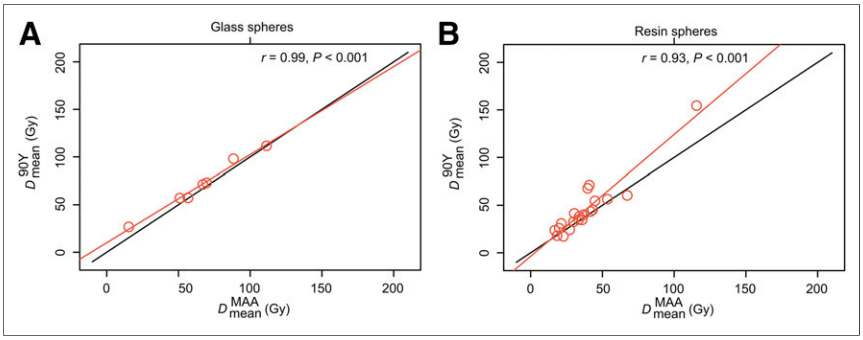

FIGURE 7. Comparison of nontumor mean dose D_{mean} between predictive ^{90}Y dosimetry based on ^{99m}Tc-MAA SPECT and posttreatment dosimetry based on ^{90}Y TOF PET for glass (A) and resin (B) spheres. Diagonal red lines indicate linear regression fitted with least-squares method; diagonal black line indicates perfect concordance.

Average ^{99m}Tc-MAA uptake in TV has been shown to depend on tumor type (*23*), and a large variation in uptake has been observed within each given tumor type. Therefore, an extension of the present work to tumor types other than HCC could be of interest.

NTV

Predictive dosimetry in NTV tended to slightly underestimate posttreatment dosimetry ($DR^{NTV}_{mean} < 1$). Quantitative agreement between predictive and posttreatment dosimetry was more accurate for NTV than for TV (lower DR^{NTV} variability), possibly because of a better overall agreement achievable in larger volumes than in smaller ones. This hypothesis is supported by Figure 6, which indicates lower DR^{NTV} variability for patients treated with glass spheres, for whom the TV/NTV ratio was also lower as shown in Supplemental Figure 4. In view of the observed low DR^{NTV} variability, we are confident that severe overdosing of the remaining functional parenchyma can be avoided, thus providing a safe treatment to the patient.

Even when agreement between predictive ^{90}Y dosimetry based on ^{99m}Tc-MAA SPECT and posttreatment dosimetry based on ^{90}Y TOF PET was good for both TV (averaged overestimation, ~30%) and NTV (averaged underestimation, ~10%), some cases of important discrepancy occurred (extreme values in Fig. 6 and Table 6).

One limitation of our study was the low number of patients treated with the glass sphere approach (7 procedures; 11 TVs).

This study concerned and compared predictive and posttreatment dosimetry for both glass sphere radioembolization and resin sphere radioembolization performed by the same team at the same institution, thus adopting uniform, repeatable radioembolization and imaging procedures. In most other published studies, resin sphere radioembolization and glass sphere radioembolization were not performed at the same institution or by the same staff. We believe our approach (unification and homogeneity of patient preparation, activity administration, imaging procedures, and data analysis) in assessing and comparing the dosimetry for the two therapeutic options helps reduce quantitative bias.

CONCLUSION

In HCC patients undergoing ^{90}Y-sphere radioembolization, we conclude that the ^{90}Y dose inferred from ^{99m}Tc-MAA SPECT/CT

TABLE 7
Lin Concordance Coefficients, in NTV, Between Predictive Dosimetry Based on ^{99m}Tc-MAA SPECT and Posttreatment Dosimetry Based on ^{90}Y TOF PET for D_{mean} and D_{70} for Both Types of Microsphere (Fig. 7)

	Precision (ρ)		Accuracy (C_b)		Concordance (ρ_c)	
Sphere type	D_{mean}	D_{70}	D_{mean}	D_{70}	D_{mean}	D_{70}
Glass	0.99	1.00	0.98	0.99	0.97	0.99
Resin	0.94	0.93	0.92	0.92	0.86	0.85

is, in both TVs and NTVs, a valuable predictor of the posttreatment ^{90}Y TOF PET/CT–derived absorbed dose. In particular, the low variability of DR^{NTV} shows promise for predicting the absorbed dose in the remaining functional parenchyma and possibly for preserving hepatic function by minimizing toxicity. Furthermore, our analysis suggests that the predictive value in NTV is better for low TV/NTV ratios. Nevertheless, a discrepancy between predictive and posttreatment dosimetry was found in specific cases, possibly because of the differences in physical properties between ^{99m}Tc-MAA and ^{90}Y-spheres, morphologic variations in hepatic or tumor vascularization, or an inability to perfectly reproduce the administration procedure. Therefore, we recommend performing post-SIRT dosimetry based on ^{90}Y TOF PET/CT, especially if fractionated treatment or dose–response/dose–toxicity studies are needed. Postradioembolization ^{90}Y TOF PET/CT can also provide valuable information in cases of extrahepatic shunt, helping the physician take appropriate corrective actions and improving posttherapy patient management.

Our study on the quantitative agreement of predictive and post-SIRT dosimetry found that, at a macroscopic level, there are no relevant differences between glass and resin spheres for TVs of 150 mL of less.

DISCLOSURE

The costs of publication of this article were defrayed in part by the payment of page charges. Therefore, and solely to indicate this fact, this article is hereby marked "advertisement" in accordance with 18 USC section 1734. No potential conflict of interest relevant to this article was reported.

REFERENCES

1. Salem R, Lewandowski RJ, Kulik L, et al. Radioembolization results in longer time-to-progression and reduced toxicity compared with chemoembolization in patients with hepatocellular carcinoma. *Gastroenterology.* 2011;140:497.e2–507.e2.
2. Sangro B, Carpanese L, Cianni R, et al. Survival after yttrium-90 resin microsphere radioembolization of hepatocellular carcinoma across Barcelona Clinic liver cancer stages: a European evaluation. *Hepatology.* 2011;54:868–878.
3. Salem R, Mazzaferro V, Sangro B. Yttrium 90 radioembolization for the treatment of hepatocellular carcinoma: biological lessons, current challenges, and clinical perspectives. *Hepatology.* 2013;58:2188–2197.
4. Kao YH, Hock Tan AE, Burgmans MC, et al. Image-guided personalized predictive dosimetry by artery-specific SPECT/CT partition modeling for safe and effective ^{90}Y radioembolization. *J Nucl Med.* 2012;53:559–566.
5. Kao YH, Steinberg JD, Tay YS, et al. Post-radioembolization yttrium-90 PET/CT: part 1—diagnostic reporting. *EJNMMI Res.* 2013;3:56.
6. Kao YH, Tan EH, Ng CE, Goh SW. Clinical implications of the body surface area method versus partition model dosimetry for yttrium-90 radioembolization using resin microspheres: a technical review. *Ann Nucl Med.* 2011;25:455–461.
7. Lau WY, Kennedy AS, Kim YH, et al. Patient selection and activity planning guide for selective internal radiotherapy with yttrium-90 resin microspheres. *Int J Radiat Oncol Biol Phys.* 2012;82:401–407.
8. Lhommel R, van Elmbt L, Goffette P, et al. Feasibility of ^{90}Y TOF PET-based dosimetry in liver metastasis therapy using SIR spheres. *Eur J Nucl Med Mol Imaging.* 2010;37:1654–1662.
9. Ulrich G, Dudeck O, Furth C, et al. Predictive value of intratumoral ^{99m}Tc-macroaggregated albumin uptake in patients with colorectal liver metastases scheduled for radioembolization with ^{90}Y-microspheres. *J Nucl Med.* 2013;54:516–522.
10. Chiesa C, Lambert B, Maccauro M, et al. Pretreatment dosimetry in HCC radioembolization with ^{90}Y glass microspheres cannot be invalidated with a bare visual evaluation of ^{99m}Tc-MAA uptake of colorectal metastases treated with resin microspheres. *J Nucl Med.* 2014;55:1215–1216.
11. Flamen P, Vanderlinden B, Delatte P, et al. Multimodality imaging can predict the metabolic response of unresectable colorectal liver metastases to radioembolization therapy with yttrium-90 labeled resin microspheres. *Phys Med Biol.* 2008;53:6591–6603.
12. Wondergem M, Smits ML, Elschot M, et al. ^{99m}Tc-macroaggregated albumin poorly predicts the intrahepatic distribution of ^{90}Y resin microspheres in hepatic radioembolization. *J Nucl Med.* 2013;54:1294–1301.
13. Kao YH. A clinical dosimetric perspective uncovers new evidence and offers new insight in favor of ^{99m}Tc-macroaggregated albumin for predictive dosimetry in ^{90}Y resin microsphere radioembolization. *J Nucl Med.* 2013;54:2191–2192.
14. Garin E, Lenoir L, Rolland Y, et al. Dosimetry based on ^{99m}Tc-macroaggregated albumin SPECT/CT accurately predicts tumor response and survival in hepatocellular carcinoma patients treated with ^{90}Y-loaded glass microspheres: preliminary results. *J Nucl Med.* 2012;53:255–263.
15. Kao YH, Steinberg JD, Tay YS, et al. Post-radioembolization yttrium-90 PET/CT: part 2—dose-response and tumor predictive dosimetry for resin microspheres. *EJNMMI Res.* 2013;3:57.
16. Kao YH, Tan AE, Lo RH, et al. Non-target activity detection by post-radioembolization yttrium-90 PET/CT: image assessment technique and case examples. *Front Oncol.* 2014;4:11.
17. Bettinardi V, Presotto L, Rapisarda E, Picchio M, Gianolli L, Gilardi MC. Physical performance of the new hybrid PETCT Discovery-690. *Med Phys.* 2011;38:5394–5411.
18. Ho S, Lau WY, Leung TW, et al. Partition model for estimating radiation doses from yttrium-90 microspheres in treating hepatic tumours. *Eur J Nucl Med.* 1996;23:947–952.
19. Pasciak AS, Bourgeois AC, Bradley YC. A comparison of techniques for ^{90}Y PET/CT image-based dosimetry following radioembolization with resin microspheres. *Front Oncol.* 2014;4:121.
20. Eckerman KF, Endo A. *MIRD: Radionuclide Data and Decay Schemes.* 2nd ed. Reston, VA: Society of Nuclear Medicine and Molecular Imaging; 2007:205.
21. Dieudonné A, Garin E, Laffont S, et al. Clinical feasibility of fast 3-dimensional dosimetry of the liver for treatment planning of hepatocellular carcinoma with ^{90}Y-microspheres. *J Nucl Med.* 2011;52:1930–1937.
22. Lin LI. A concordance correlation coefficient to evaluate reproducibility. *Biometrics.* 1989;45:255–268.
23. Ilhan H, Goritschan A, Paprottka P, et al. Systematic evaluation of tumoral ^{99m}Tc-MAA uptake using SPECT and SPECT/CT in 502 patients before ^{90}Y radioembolization. *J Nucl Med.* 2015;56:333–338.